processes

MDPI

Article

Molecular Dynamics Unveiled: Temperature–Pressure–Coal Rank Triaxial Coupling Mechanisms Governing Wettability in Gas–Water–Coal Systems

Lixin Zhang [1,2,3], Songhang Zhang [1,2,3,*], Shuheng Tang [1,2,3], Zhaodong Xi [1,2,3], Jianxin Li [1,2,3], Qian Zhang [1,2,3], Ke Zhang [1,2,3] and Wenguang Tian [4]

[1] School of Energy Resources, China University of Geosciences (Beijing), Beijing 100083, China; zhanglx@email.cugb.edu.cn (L.Z.); tangsh@cugb.edu.cn (S.T.); xizhaod@cugb.edu.cn (Z.X.); lijianxin258@126.com (J.L.); zhangqian@email.cugb.edu.cn (Q.Z.); zhangke9801@163.com (K.Z.)
[2] Coal Reservoir Laboratory of National Engineering Research Center of CBM Development & Utilization, Beijing 100083, China
[3] Beijing Key Laboratory of Unconventional Natural Gas Geological Evaluation and Development Engineering, Beijing 100083, China
[4] Research Institute of Petroleum Exploration and Development, PetroChina, Beijing 100083, China; tianwg69@petrochina.com.cn
* Correspondence: zhangsh@cugb.edu.cn

Abstract

Water within coal reservoirs exerts dual effects on methane adsorption–desorption by competing for adsorption sites and reducing permeability. The bound water effect, caused by coal wettability, significantly constrains coalbed methane (CBM) production, rendering investigations into coal wettability crucial for efficient CBM development. Compared with other geological formations, coals are characterized by a highly developed microporous structure, making the CO_2 sequestration mechanism in coal seams closely linked to the microscale interactions among gas, water, and coal matrixes. However, the intrinsic mechanisms remain poorly understood. In this study, molecular dynamics simulations are employed to investigate the wettability behaviors of CO_2, CH_4, and water on different coal matrix surfaces under varying temperature and pressure conditions, for coal macromolecules representative of four coal ranks. The study reveals the evolution of water wettability in response to CO_2 and CH_4 injection, identifies wettability differences among coal ranks, and analyzes the microscopic mechanisms governing wettability. The results show the following: (1) The contact angle increases with gas pressure, and the variation in wettability is more pronounced in CO_2 environments than in CH_4. As pressure increases, the number of hydrogen bonds decreases, while the peak gas density of CH_4 and CO_2 increases, leading to larger contact angles. (2) Simulations under different temperatures for the four coal ranks indicate that temperature has minimal influence on low-rank Hegu coal, whereas for higher-rank coals, gas adsorption on the coal surface increases, resulting in reduced wettability. Interfacial tension analysis further suggests that higher temperatures reduce water surface tension, cause dispersion of water molecules, and consequently improve wettability. Understanding the wettability variations among different coal ranks under variable pressure–temperature conditions provides a fundamental model and theoretical basis for investigating deep coal seam gas–water interactions and CO_2 geological sequestration mechanisms. These findings have significant implications for the advancement of CO_2-ECBM technology.

check for updates

Academic Editor: Andrew S. Paluch

Received: 16 June 2025
Revised: 3 July 2025
Accepted: 9 July 2025
Published: 10 July 2025

Citation: Zhang, L.; Zhang, S.; Tang, S.; Xi, Z.; Li, J.; Zhang, Q.; Zhang, K.; Tian, W. Molecular Dynamics Unveiled: Temperature–Pressure–Coal Rank Triaxial Coupling Mechanisms Governing Wettability in Gas–Water–Coal Systems. *Processes* **2025**, *13*, 2209. https://doi.org/10.3390/pr13072209

Copyright: © 2025 by the authors. Licensee MDPI, Basel, Switzerland. This article is an open access article distributed under the terms and conditions of the Creative Commons Attribution (CC BY) license (https://creativecommons.org/licenses/by/4.0/).

Keywords: coal rank; wettability; temperature and pressure conditions; molecular dynamics simulation

1. Introduction

In situ coal reservoirs constitute a complex coal–gas–water system, comprising methane that exists in both adsorbed and free states [1], as well as water distributed in adsorbed, capillary-bound, and free forms [2]. The injection of gases such as N_2 or CO_2 during coalbed methane (CBM) development for enhanced recovery or CO_2 sequestration further complicates the composition of gases within the coal matrix. These system components are intricately coupled via competitive adsorption, wettability, and multiphase flow dynamics. Among these, wettability is a critical factor influencing the complex interactions within the coal–water–gas system, affecting strategies for reservoir protection, permeability enhancement, and optimization of gas and water transport [3–6]. Therefore, understanding coal reservoir wettability and elucidating the mechanisms of coal–gas–water interactions are not only essential for guiding CBM production [7–10] but also for advancing clean coal utilization and CO_2 geological storage under the "dual carbon" (carbon peaking and neutrality) strategy [11–14].

Historically, research on coal wettability has primarily focused on experimental studies involving coal composition and surface chemical structure [15–19]. Physical experiments have shown that wettability is sensitive to variations in reservoir pressure and temperature. Zheng et al. [4], utilizing nuclear magnetic resonance (NMR), investigated the effects of pressure, temperature, and water state on CO_2-H_2O wettability during the CO_2-ECBM process, comparing results for subbituminous and anthracite coals. Their results showed that CO_2 wettability significantly increased with rising CO_2 injection pressure, stabilizing at 5 MPa, and that lower temperatures further enhanced CO_2 wettability. Similarly, Sun et al. [3] found that low temperatures and high CO_2 pressures both promote enhanced wettability of coal to CO_2. Siemons et al. [20] explored contact angle changes in an anthracite–water–CO_2 system, concluding that at 45 °C and above 2.6 bar, water became the non-wetting phase. Chen et al. [21] employed low-field NMR to test the effect of CO_2 and He on the wettability of low-rank coals, confirming that CO_2 significantly alters coal wettability with increasing pressure, while helium had no such effect. Despite these advances, physical experiments are often labor-intensive and limited to the influence of single factors such as temperature or pressure, and typically operate under lower-than-reservoir P–T conditions due to equipment constraints.

With advances in computational technologies, molecular simulations have increasingly been applied to investigate the microscopic mechanisms of coal surface wettability [22,23]. Zhao et al. [24] revealed the effects of carbon and oxygen content on the wettability of coal dust via molecular simulations of three bituminous coal samples from the Pingdingshan mining area. Li et al. [25] constructed coal surface models with various oxygen-containing functional groups based on the Wiser molecular structure and demonstrated that hydroxyl groups exhibit superior hydration behavior. Meng et al. [26] analyzed the wettability of coals at different metamorphic stages through molecular simulations and elucidated the effects of surfactant types based on adsorption sites and spacing. Xia et al. [27] investigated polar and non-polar molecule interactions during coal flotation by simulating graphene surfaces modified with oxygenated groups. Yao et al. [6] simulated wettability behavior of two oxygen-functionalized coal molecules under different temperature and pressure conditions using molecular dynamics. However, existing molecular simulations are often limited in terms of the diversity and accuracy of coal macromolecular models used. Liu [28],

through contact angle measurements of CO_2 and N_2 under different pressures and temperatures, confirmed that the phase behavior of CO_2 influences its competitive wettability with water, and that supercritical CO_2 exhibits significantly greater surface reactivity than N_2. Nevertheless, many prior studies adopt outdated classical coal models or simplified oxygen-functionalized graphene surfaces. Some works rely on a single molecular model while adjusting only the quantity of surface oxygen groups. Zhang et al. [29] constructed a molecular model sequence for 13 coals, with vitrinite reflectance (Ro) ranging from 0.46% to 3.21% using proximate and ultimate analysis, NMR, FTIR, and XPS data—offering a solid foundation for cross-rank molecular simulation studies.

In this study, planar molecular models were constructed based on four coal ranks from the eastern margin of the Ordos Basin and the Qinshui Basin, with vitrinite reflectance ranging from 0.67% to 2.21%. Molecular dynamics simulations were conducted to evaluate wettability in CH_4 and CO_2 environments under reservoir conditions (temperature: 20–60 °C; pressure: 2.5–10 MPa). The objective is to investigate the wettability characteristics of in situ coal reservoirs, reveal the microscale interaction mechanisms within coal–gas–water systems, and provide a theoretical basis for CBM development and CO_2-ECBM engineering design in the Ordos and Qinshui basins.

2. Molecular Models and Research Methods

2.1. Molecular Models

The coal macromolecular structure model forms the fundamental basis for all simulation efforts. In this study, four representative coal macromolecular models were selected from the structural sequence proposed in reference [29], which encompasses Ro values ranging from 0.46% to 3.21%. The selected models represent coal ranks with Ro values between 0.67% and 2.21%. These four models correspond to coals sampled from different locations and ranks: Hequ (HQ) coal (long-flame coal), Dianping (DP) coal (coking coal), Gaoyang (GY) coal (lean coal), and Zhaozhuang (ZZ) coal (semi-anthracite). Their respective molecular formulas are $C_{214}H_{189}N_3O_{34}S$, $C_{207}H_{170}O_3N_2S$, $C_{199}H_{139}O_3N_3S_2$, and $C_{204}H_{157}O_5N_3$.

The sampling locations, spatial distribution, and molecular characteristics of the selected coals are shown in Figure 1 and detailed in Tables 1–3. These four coal samples span a wide range of coalification stages and effectively represent the evolutionary trends of wettability across different coal ranks under varying pressure–temperature conditions in the study areas.

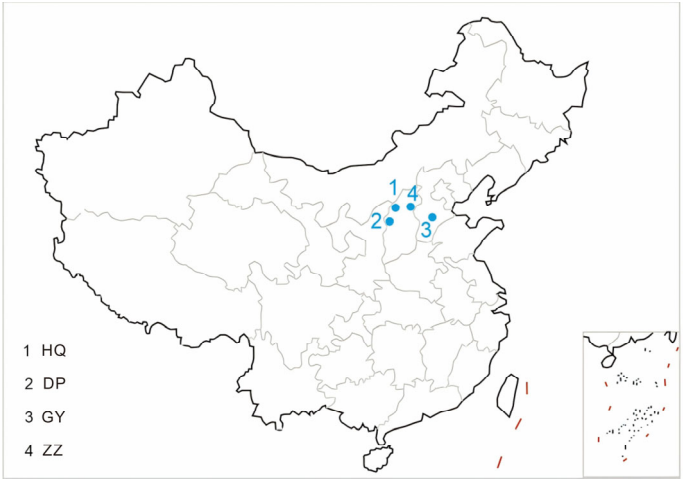

Figure 1. Coal sample collection point diagram.

Table 1. Information on coal samples.

No.	Sample	Sampling Site	Stratigraphy	Sedimentary Environment
1	HQ	Hequ coal mine	Permian Taiyuan formation	Fluvial-deltaic plain deposition
2	DP	Dianping coal mine	Permian lower Shihezi formation	Meandering delta plain deposition
3	GY	Gaoyang Coal mine	Carboniferous-Permian Taiyuan formation	Barrier-lagoon deposition
4	ZZ	Zhaozhuang Coal mine	Carboniferous-permian Taiyuan formation	Lagoon deposition

Table 2. Statistical distribution of oxygen-containing functional groups in coals of different ranks.

Sample	R_O (%)	Carbonyl	Carboxyl	Hydroxyl	Ether Oxygen	Aldehyde
HQ	0.67	2	2	28	2	0
DP	1.50	0	0	2	0	1
GY	1.96	1	0	1	1	0
ZZ	2.21	1	0	1	3	0

Table 3. Hydrogen bond statistics for coals of different ranks.

Sample	R_O (%)	Total H-Bonds	Intra-Coal H-Bonds	Intra-Water H-Bonds	Interfacial H-Bonds
HQ	0.67	909	199	625	85
DP	1.50	702	4	694	4
GY	1.96	698	0	692	6
ZZ	2.21	698	2	685	11

2.2. Research Methods

Wettability testing of coal is typically performed on flat coal surfaces; thus, prior to simulating water wettability, it is necessary to construct slab models of coal macromolecules. Simultaneously, a spherical water droplet model must be generated to form the coal–water system. The procedures for constructing the coal slab model and coal–water system, along with parameter settings and model optimization in Materials Studio (MS) 9.0 software, are detailed in reference [30]. The spherical water droplet was constructed with a density of 1 g/cm^3, composed of 500 water molecules and a radius of 15 Å. For consistency across simulations, the size of each coal slab model was fixed at 90 × 65 Å, with a thickness of 17 Å—sufficient to ensure full spreading of the droplet and satisfy the wettability simulation requirements. The fixed dimensions were chosen based on fundamental physical constraints and computational best practices documented in the coal-wettability literature [22,24,30,31].

Due to variations in density across coal ranks, the number of coal molecules included in each slab model varies slightly, but each contains approximately 25 molecules. After model construction, molecular dynamics (MD) simulations were performed using the Dynamic task within the Forcite module. Given the intermediate scale of the coal–water system, the NVT ensemble was applied. The simulations used the Nosé thermostat for temperature control, the COMPASSII force field, particle–particle particle–mesh (PPPM) for long-range electrostatic interactions, and the atom-based method for van der Waals forces. The time step was set to 1 fs, and the total simulation time was 800 ps.

To evaluate the influence of model size, water droplet composition, and simulation parameters on wettability outcomes, a sensitivity analysis was conducted. For the slab size, expanding the dimensions to 120 × 80 Å (as referenced in reference [30]) induced negligible changes in contact angles, which aligns with prior studies [22] showing that lateral dimensions exceeding 70 Å can mitigate edge effects. Concerning the droplet size, varying the number of molecules from 300 to 1000 (consistent with the 500-molecule standard in coal–gas simulations [31]) demonstrated minimal size-dependent effects, as smaller droplets

may lead to statistical noise, and larger ones may compromise computational efficiency. Switching to the ReaxFF force field (as used in reference [25] for covalent bond analysis) introduced minor quantitative shifts in contact angles but preserved the qualitative trends, thus validating the robustness of the COMPASSII force field. Temperature control using either the Nosé or Andersen thermostats (both commonly used in NVT ensemble simulations [24]) yielded consistent results, confirming that the thermal management protocols had no significant impact on the wettability metrics.

To investigate the effect of pressure on coal surface wettability across different coal ranks, coal–gas–water models were constructed at 298 K under varying pressures. Amorphous CO_2 and CH_4 cells at 2.5, 5.0, 7.5, and 10.0 MPa were generated using the Amorphous Cell module in MS and subsequently introduced into each coal–water system (see Figure 2, which shows the HQ coal–CO_2–water system at 5.0 MPa as an example). These combined systems were used to evaluate contact angles on coal surfaces at different pressures and gas environments, enabling assessment of the impact of pressure and gas type on wettability. Building on this pressure–wettability analysis, the HQ coal model was further used to examine the molecular density distributions of CH_4-H_2O and CO_2-H_2O under pressures of 2.5, 5.0, 7.5, and 10.0 MPa. This analysis provided molecular-level insights into the mechanisms by which different gases influence wettability behavior on coal surfaces.

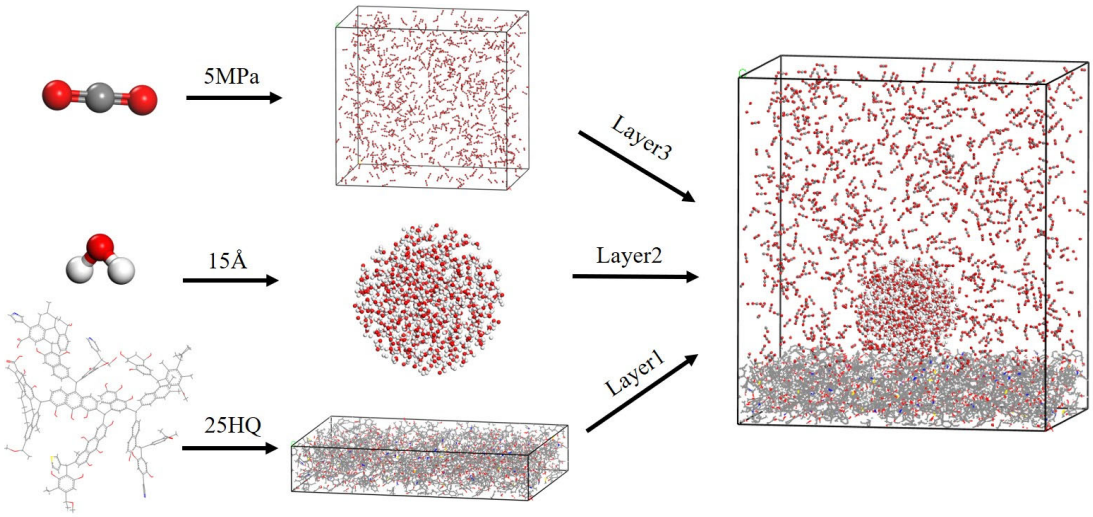

Figure 2. Establishment of the coal–gas–water system (HQ coal in 5 MPa, CO_2 environment).

To investigate the influence of temperature on coal surface wettability across different coal ranks, CO_2 and CH_4 gases were injected into the coal–water systems at a constant pressure of 5 MPa. The system temperatures were set to 298 K, 318 K, and 338 K, respectively. Molecular dynamics (MD) simulations were performed to calculate the corresponding contact angles, enabling analysis of the temperature-dependent wettability behavior under different gas environments. Based on the temperature–wettability analysis, further investigation was conducted on the density distributions of CO_2 and CH_4 molecules along the *Z*-axis at 298 K, 318 K, and 338 K for each coal rank. A Cartesian coordinate system was established with the base of the coal slab defined as the XY plane and the vertical direction as the *Z*-axis (as illustrated in Figure 2). This spatial configuration facilitates detailed analysis of molecular density profiles in the coal–water–CH_4 and coal–water–CO_2 systems.

3. Simulation Results

3.1. Wettability of Coal Under Different Pressures

Wettability simulations were conducted using coal–gas–water systems at a constant temperature of 298 K under varying pressure conditions. Contact angles on the coal surfaces were measured for different coal ranks under CO_2 and CH_4 environments, allowing evaluation of the influence of pressure on coal wettability across different gas types.

The results of contact angle measurements for different coal ranks under varying pressure conditions are shown in Figures 3–6. To better visualize the changes in contact angles, CO_2 and CH_4 gas molecules were omitted from the figures.

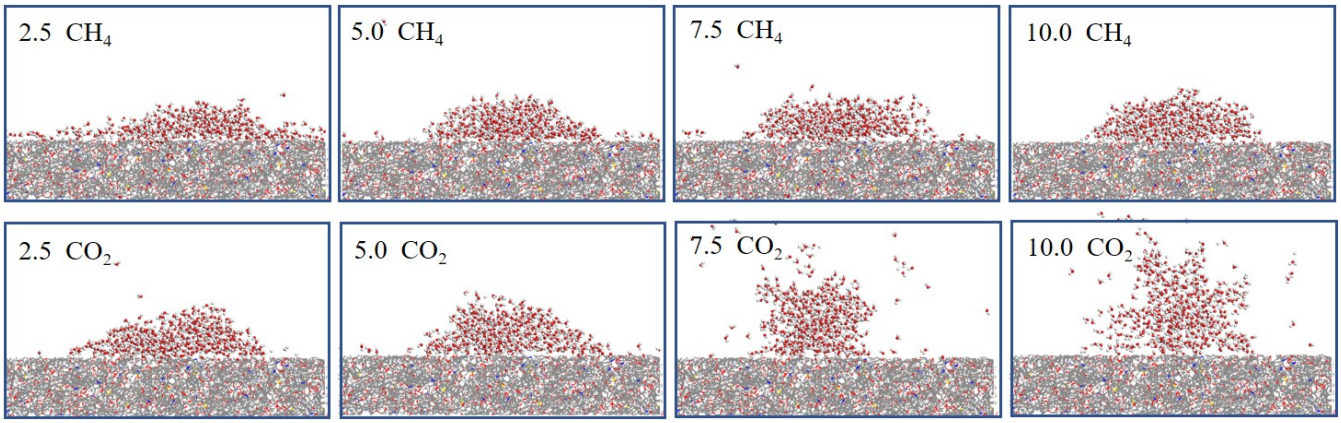

Figure 3. Contact angles of HQ coal under different pressure conditions.

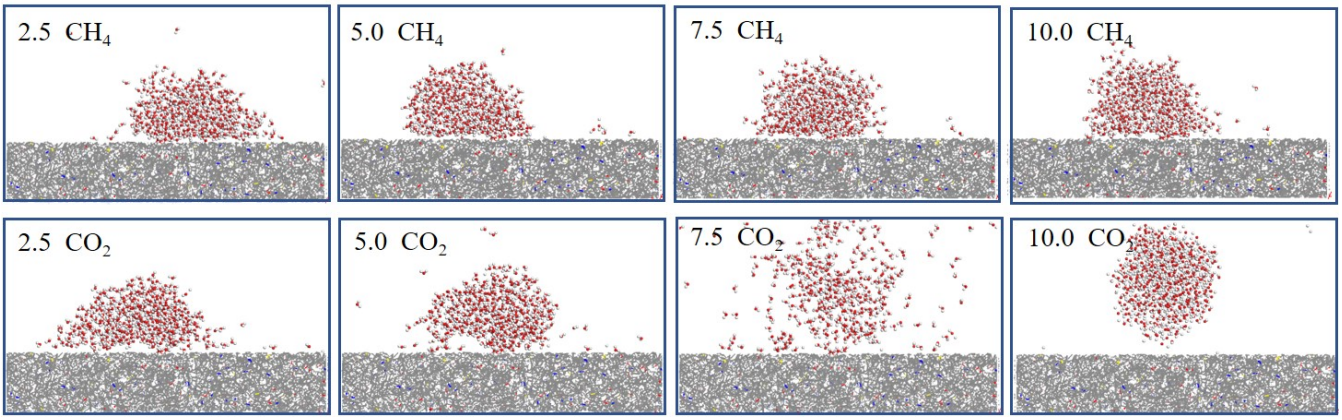

Figure 4. Contact angles of DP coal under different pressure conditions.

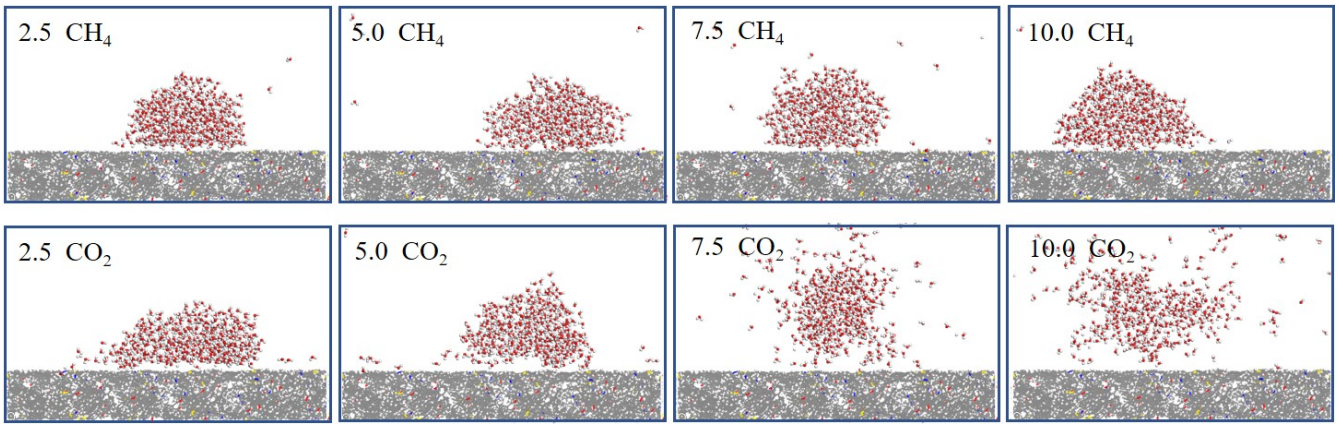

Figure 5. Contact angles of GY coal under different pressure conditions.

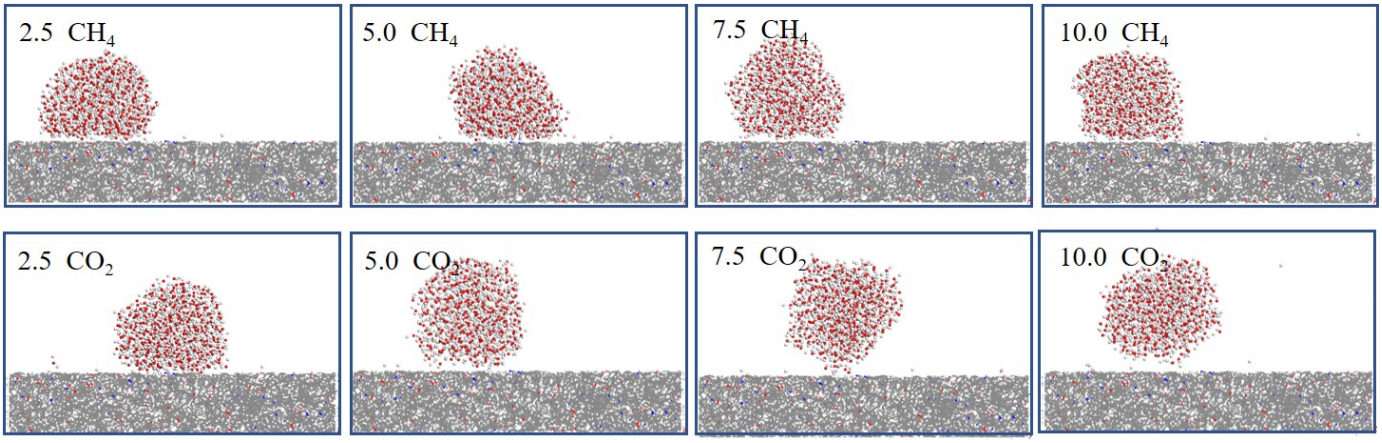

Figure 6. Contact angles of ZZ coal under different pressure conditions.

The final contact angle was determined as the average of the contact angles measured on the XZ and YZ planes of the coal–gas–water system. The contact angles obtained under different pressure conditions for various coal ranks are summarized in Table 4 and illustrated in Figure 7. In the coal–water–methane systems at a constant temperature of 298 K and pressures ranging from 2.5 to 10.0 MPa, with coal ranks corresponding to Ro values between 0.67% and 2.21%, the measured water contact angles ranged from 32.92° to 89.78°. Overall, the coals exhibited water-wet behavior, with contact angles increasing as both pressure and coal rank increased. However, the rate of increase in contact angle with pressure decreased with rising coal rank. Under identical conditions, the coal–water–CO_2 systems exhibited contact angles ranging from 33.81° to 136.37°, also showing a positive correlation with both gas pressure and coal rank. Notably, at the same temperature and pressure, contact angles in the coal–water–CH_4 systems were consistently lower than those in the coal–water–CO_2 systems. Additionally, a distinct wettability reversal was observed in the CO_2 systems; for several high-rank coals, the contact angles exceeded 90° when the pressure surpassed 5 MPa, indicating a transition from water-wet to gas-wet behavior.

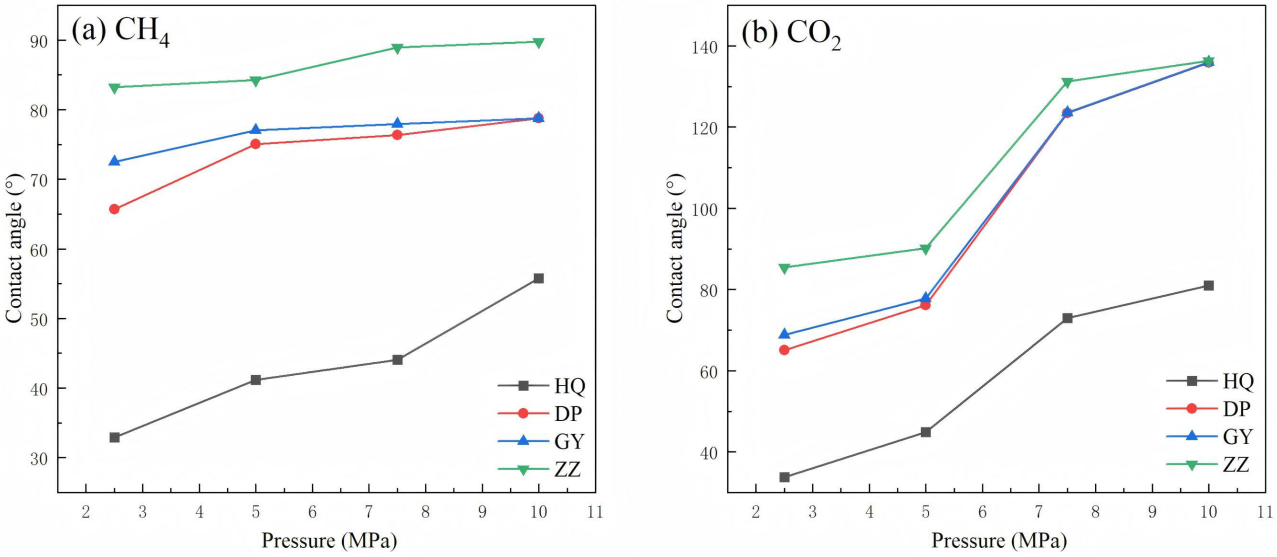

Figure 7. Changes in contact angles under different gas pressure conditions. (**a**) CH_4 gas pressure; (**b**) CO_2 gas pressure.

Table 4. Changes in contact angles of different coals under different environmental conditions.

Sample	CH_4 Environment				CO_2 Environment			
	2.5 Mpa	5.0 Mpa	7.5 Mpa	10.0 Mpa	2.5 Mpa	5.0 Mpa	7.5 Mpa	10.0 Mpa
HQ	32.92° ± 2.1°	41.17° ± 2.3°	44.07° ± 2.5°	55.74° ± 2.8°	33.81° ± 2.0°	44.90° ± 2.4°	72.91° ± 2.7°	81.02° ± 2.9°
DP	65.71° ± 2.5°	75.02° ± 2.6°	76.34° ± 2.7°	78.75° ± 2.8°	65.10° ± 2.4°	76.09° ± 2.5°	123.48° ± 2.7°	135.86° ± 2.8°
GY	72.51° ± 2.6°	77.03° ± 2.7°	77.94° ± 2.7°	78.78° ± 2.8°	68.82° ± 2.5°	77.73° ± 2.6°	123.54° ± 2.7°	135.95° ± 2.8°
ZZ	83.24° ± 2.8°	84.24° ± 2.8°	88.96° ± 2.9°	89.78° ± 2.9°	85.47° ± 2.7°	90.15° ± 2.8°	131.28° ± 2.9°	136.37° ± 3.0°

Notes: Errors represent standard deviations from five independent simulations with randomized initial configurations. Wettability reversal (e.g., DP coal in CO_2 at 10.0 MPa) is confirmed by non-overlapping error ranges between consecutive pressure points (e.g., 76.09 ± 2.5° at 5.0 MPa vs. 135.86 ± 2.8° at 10.0 MPa; $p < 0.01$, two-tailed *t*-test). Error magnitudes correlate with coal rank heterogeneity (higher rank—larger uncertainty).

3.2. Wettability of Coal Under Different Temperatures

At a constant pressure of 5 MPa, the wettability of coals with different ranks was evaluated at temperatures of 298 K, 318 K, and 338 K. The corresponding contact angle results are summarized in Table 5 and illustrated in Figure 8.

Table 5. Contact angle statistics for coal surfaces of different ranks under CH_4 and CO_2 environments at constant pressure (5 MPa).

Sample	R_O (%)	Contact Angle (CH_4, 5 MPa) (°)			Contact Angle (CO_2, 5 MPa) (°)		
		298 K	318 K	338 K	298 K	318 K	338 K
HQ	0.67	41.17	40.75	40.34	44.90	44.34	43.75
DP	1.50	75.02	63.73	58.08	76.09	63.34	59.64
GY	1.96	77.03	66.74	62.08	77.73	74.90	71.51
ZZ	2.21	84.24	75.38	73.18	90.15	83.09	79.82

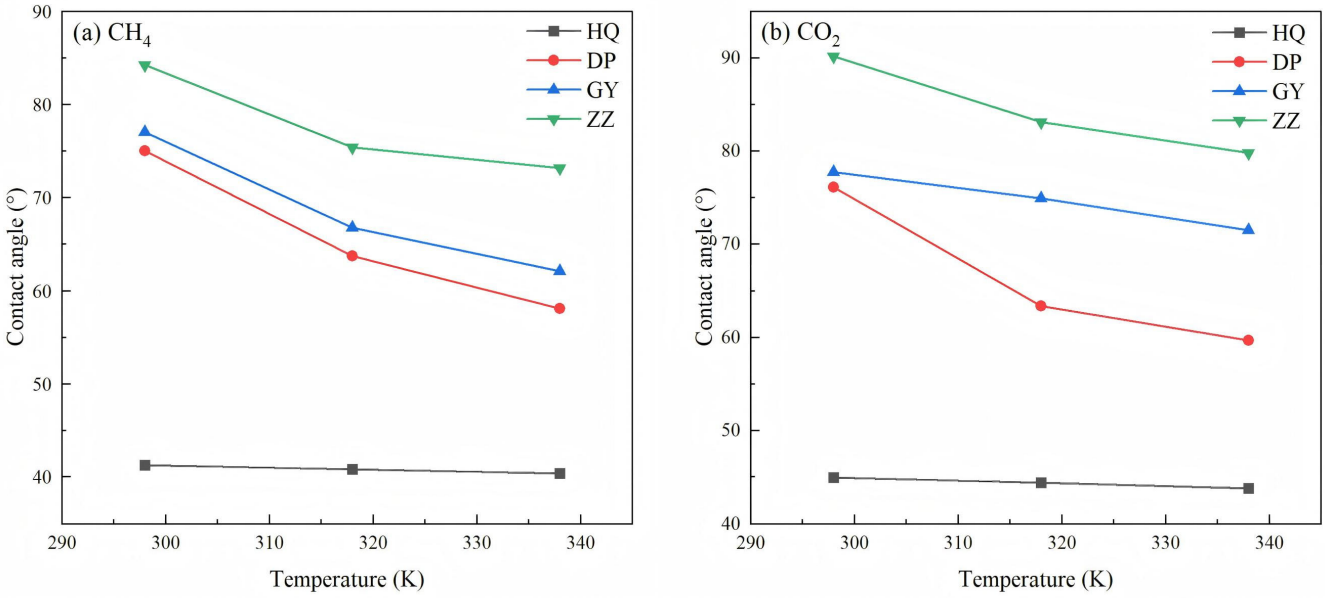

Figure 8. Changes in contact angles under different gas temperature conditions. (**a**) CH_4 gas pressure; (**b**) CO_2 gas pressure.

As shown in Table 5, for the coal–water–CH_4 systems at a constant pressure of 5 MPa and temperatures ranging from 298 K to 338 K, with coal ranks corresponding to Ro values between 0.67% and 2.21%, the water contact angle varied from 84.24° to 40.34°. Overall, the coals exhibited water-wet behavior. The contact angle generally decreased with increasing temperature and coal rank. Moreover, the sensitivity of contact angle to temperature increased with coal rank; low-rank coals showed minimal change, while

higher-rank coals exhibited a more pronounced temperature-dependent reduction. Under identical conditions, the coal–water–CO_2 systems displayed contact angles ranging from 90.15° to 43.75°, also demonstrating a decreasing trend with increasing temperature and coal rank. At the same pressure and temperature, the contact angles in CH_4 systems were consistently lower than those in CO_2 systems. As illustrated in Figure 8, the difference in contact angle between 298 K and 338 K is relatively small at 5 MPa for both CO_2 and CH_4 environments. However, with increasing coal rank, the variation in contact angle becomes more apparent. Specifically, low-rank coals exhibit negligible change, mid-rank coals show the most significant reduction, and high-rank coals fall between the two extremes (Figure 9).

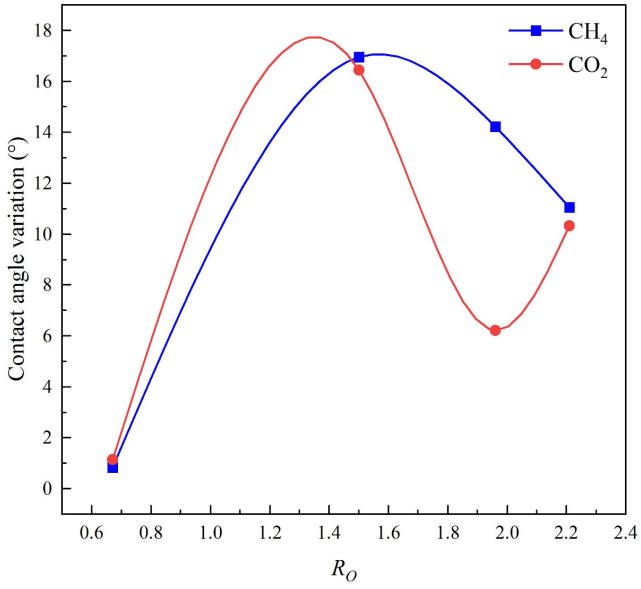

Figure 9. Variation in contact angle difference under different gas environments.

4. Discussion

4.1. Effect of Pressure on Coal Wettability

Simulation results under varying pressure conditions indicate that contact angles in pressurized gas environments are higher than the original (baseline) values, suggesting that increased pressure reduces coal surface wettability. Similar findings were reported by Si Binbin et al. [32], who used a molecular model of anthracite and observed through molecular simulations that coal wettability progressively weakens with increasing gas pressure. Yue Jiwei et al. [33] developed an experimental setup to measure coal–water contact angles under CH_4 atmospheres and found that the contact angle increased with pressure. These conclusions are consistent with the results of this study. As pressure increases, gas density correspondingly rises, leading to enhanced gas adsorption on the coal surface due to competitive adsorption effects. A dense layer of gas molecules forms on the coal surface, occupying adsorption sites that would otherwise be available to water molecules. As a result, the contact angle increases and the coal becomes less wettable (Figure 10).

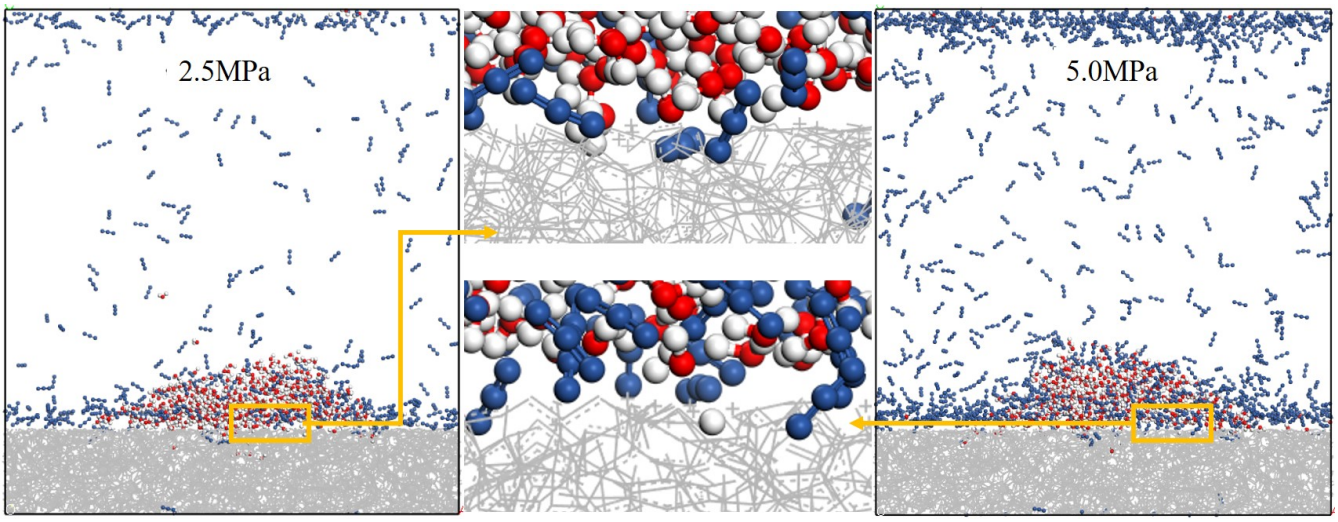

Figure 10. Detailed view of the HQ coal surface under different pressures (blue represents CO_2 molecules).

Based on the coal–gas–water models at 298 K under varying pressures, the number of hydrogen bonds formed between water molecules and coal surfaces was quantified for different coal ranks. Hydrogen bonds were identified according to geometric criteria: a donor–acceptor distance less than 0.25 nm and a donor–hydrogen–acceptor angle greater than 135° were considered indicative of hydrogen bonding. The results under different pressure conditions for each coal rank are summarized in Table 6. Overall, regardless of whether the gas environment was CH_4 or CO_2, the number of hydrogen bonds between water and the coal surface decreased with increasing gas pressure. This decline was most pronounced in the low-rank HQ coal system, while in the medium- and high-rank DP, GY, and ZZ coal systems, the variation was less significant. Under the same pressure conditions, CH_4 environments consistently exhibited a greater number of hydrogen bonds between water and coal surfaces compared to CO_2 environments. Notably, under 10 MPa pressure, zero hydrogen bonds were observed in the high-rank coal–water–CO_2 systems. This observation provides a clear mechanistic explanation for the wettability reversal discussed earlier, where high-rank coals exhibited contact angles exceeding 90° at pressures above 5 MPa in CO_2 environments—indicating a transition from water-wet to gas-wet behavior.

Table 6. Number of hydrogen bonds formed between water and coal surfaces under different pressure conditions and gas environments.

Sample	R_O (%)	CH_4 Environment (Number of H-Bonds)				CO_2 Environment (Number of H-Bonds)			
		2.5 MPa	5.0 MPa	7.5 MPa	10.0 MPa	2.5 MPa	5.0 MPa	7.5 MPa	10.0 MPa
HQ	0.67	147	84	92	56	83	74	31	21
DP	1.50	8	6	6	5	6	2	2	0
GY	1.96	15	10	12	6	14	9	5	0
ZZ	2.21	11	8	6	4	9	6	2	0

As gas pressure increases, gas molecules exhibit enhanced adsorption onto the coal surface, occupying the adsorption sites that would otherwise be available to water molecules. This hinders the approach of water molecules to the surface or prevents them from adopting configurations favorable for hydrogen bond formation. Additionally, at high pressures, gas molecules may penetrate into coal pores and displace pore water, further reducing the number of hydrogen bonds. Hydrogen bonds strengthen the interaction between water molecules and the solid surface, promoting droplet spreading and resulting in smaller

contact angles—indicative of stronger hydrophilicity. Therefore, as the number of hydrogen bonds decreases, droplet spreading becomes less favorable, leading to larger contact angles and reduced wettability.

4.2. Analysis of Wettability Differences Caused by Different Gases

Simulation results under different temperature conditions reveal that, regardless of whether the environment is CO_2 or CH_4, the contact angle decreases with increasing temperature. This trend can be attributed to the enhanced kinetic energy of water molecules at higher temperatures, which facilitates faster diffusion and distribution across the coal surface. Simultaneously, the increased kinetic energy of gas molecules raises their probability of desorption, leading to a reduction in the amount of CO_2 and CH_4 adsorbed on the coal surface. As a result, more adsorption sites become available for water molecules, allowing them to approach the coal surface more easily and form hydrogen bonds. The increased number of hydrogen bonds promotes better wetting, resulting in smaller contact angles and improved coal wettability. To further explore the molecular mechanism behind this phenomenon, density profiles of CO_2 and CH_4 molecules along the *Z*-axis were analyzed for different coal ranks at various temperatures under a fixed pressure of 5 MPa (Figures 11–14). These analyses provide molecular-level insights into how temperature influences wettability differences across coal ranks.

As shown in Figures 11–14, the gas density distribution curves for all coal ranks exhibit two distinct peaks. The first peak represents the gas density near the coal matrix surface, while the second corresponds to the gas density under periodic boundary conditions. The peak values of CO_2 and CH_4 density along the *Z*-axis at 298 K, 318 K, and 338 K were statistically analyzed and are summarized in Table 7. According to Table 7, as temperature increases, the CO_2 density in the HQ coal–CO_2–water system decreases from 0.798 g/cm^3 to 0.748 g/cm^3. Although the density decreases, the reduction is relatively minor. Similarly, in the HQ coal–CH_4–water system, CH_4 density decreases from 0.102 g/cm^3 to 0.056 g/cm^3 with increasing temperature, again showing a relatively small decline. In contrast, for the other coal samples, the gas density decreases more significantly with rising temperature, and the degree of reduction increases with higher Ro values. This trend indicates that elevated temperature reduces gas adsorption on the coal surface, thereby improving coal wettability. Moreover, the greater the reduction in gas density, the larger the corresponding change in contact angle. Overall, the decrease in gas density—and thus the enhancement in wettability—is more pronounced in CO_2 environments than in CH_4 environments.

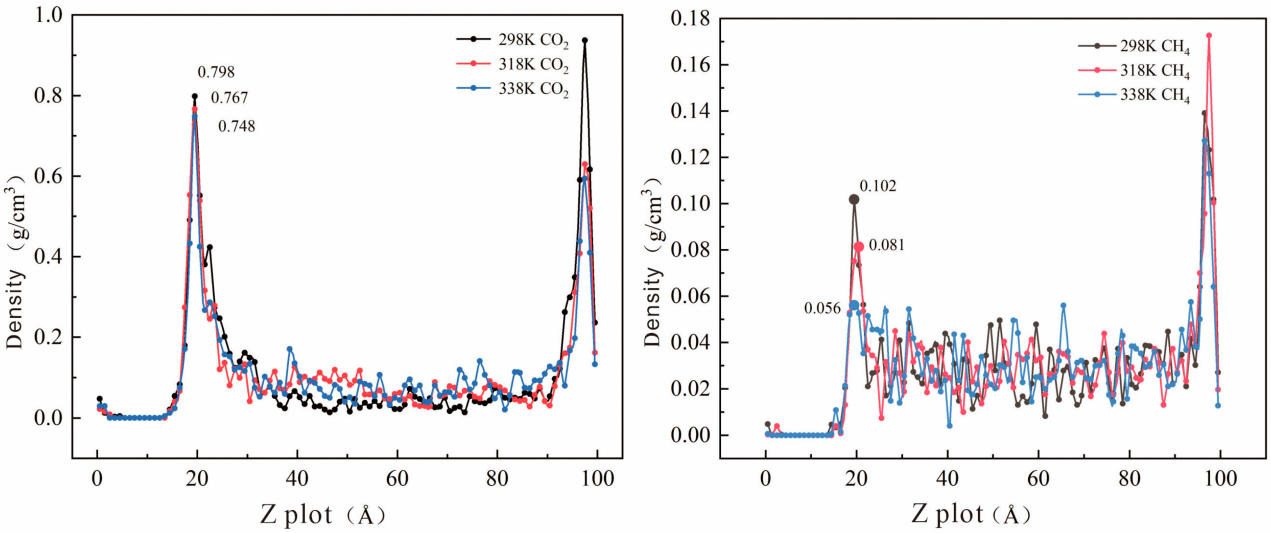

Figure 11. Gas density distribution on the surface of HQ coal at different temperatures.

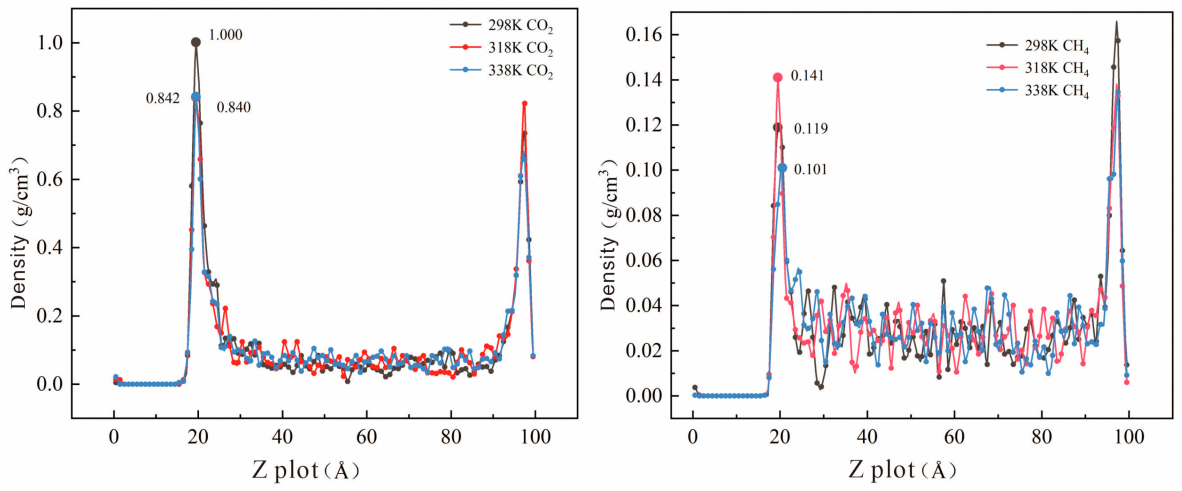

Figure 12. Gas density distribution on the surface of DP coal at different temperatures.

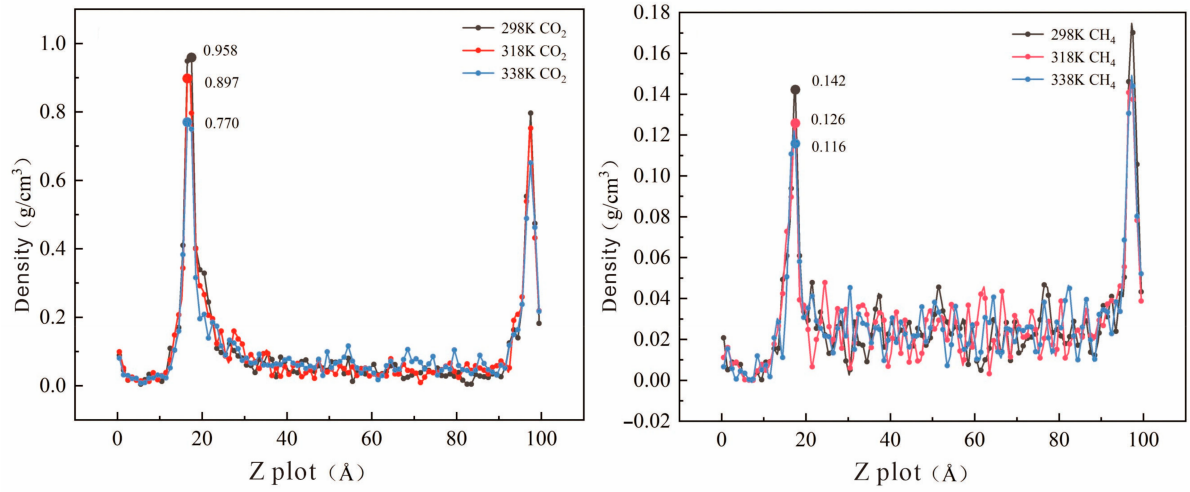

Figure 13. Gas density distribution on the surface of GY coal at different temperatures.

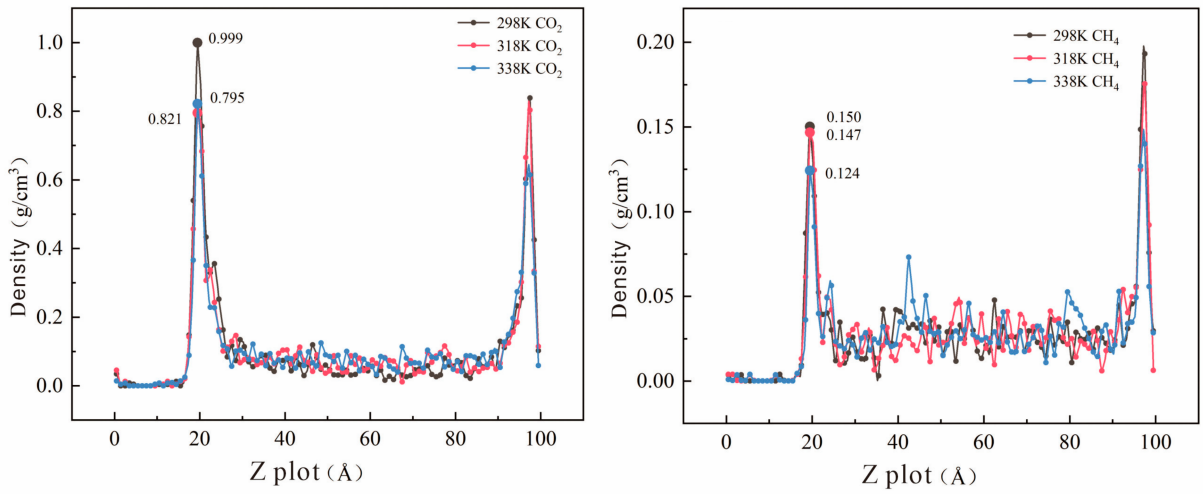

Figure 14. Gas density distribution on the surface of ZZ coal at different temperatures.

Table 7. Peak gas densities on coal surfaces under different temperature conditions at constant pressure (5 MPa).

Sample	R_O (%)	CO_2 Density Peak (g/cm^3)			CH_4 Density Peak (g/cm^3)		
		298 K	318 K	338 K	298 K	318 K	338 K
HQ	0.67	0.798	0.767	0.748	0.102	0.081	0.056
DP	1.50	1.000	0.842	0.840	0.141	0.119	0.101
GY	1.96	0.958	0.897	0.770	0.142	0.126	0.116
ZZ	2.21	0.999	0.821	0.795	0.150	0.147	0.124

In the simulation experiment, temperature increase causes the contact angle of the coal surface in the CO_2 environment to increase. According to the improvement of the Owens and Wendt polar liquid decline trend model by Vella [6], use Equations (1) and (2) to calculate the contact angle.

$$\cos(\theta) = -1 + \frac{2}{\sqrt{\gamma_{LV,0}(1 - aT)}}\sqrt{c}(20^\circ < T < 90^\circ) \quad (1)$$

$$C = \sqrt{\gamma_{SL}^{D}\frac{\gamma_{AL}^{D}}{\gamma_{AL}} + \gamma_{SL}^{P}\frac{\gamma_{AL}^{P}}{\gamma_{AL}}} \quad (2)$$

where θ is the static contact angle, $\gamma_{LV,0}$ is the surface tension of water at 20 °C, a is the temperature coefficient, c is calculated by Equation (2), γ_{SL}^{D} is solid–liquid interfacial tension, γ_{AL}^{D} and γ_{AL}^{P} are those of the air–liquid interfacial tension, γ_{AL} is the total air–liquid surface tension, and D and P are the separation force and the combination force, respectively.

In the contact angle calculation formula, temperature T is the only variable. When T increases, cos(θ) increases, and the corresponding θ decreases.

For the intermolecular forces between H_2O and CO_2 on the coal matrix surface, as shown in Figure 15, when the pressure is constant (5 MPa), the increase in temperature leads to an increase in the distance between molecules. Therefore, the attraction between the outermost molecules on the water droplet surface and other molecules decreases; that is, FH_2O-H_2O becomes smaller, and the surface tension of water decreases. Similarly, the increase in temperature also causes a decrease in the interaction force between CO_2 and H_2O (FCO_2-H_2O), leading to a decrease in the surface tension of H_2O-CO_2. Due to the decrease in the surface tension of water, the force that maintains the liquid droplet shape becomes weaker, the water molecules disperse, which leads to a decrease in the wetting angle and an improvement in wettability.

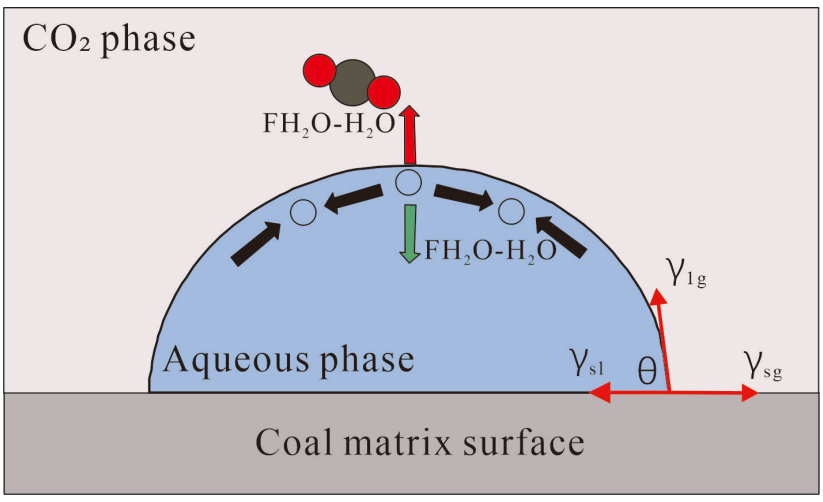

Figure 15. Intermolecular forces between H_2O and CO_2 on the coal matrix surface.

4.3. Comparative Analysis of CH_4 and CO_2 Effects on Coal Wettability

As shown in Figure 10, under CH_4 and low-pressure CO_2 environments (2.5 MPa and 5.0 MPa), gas molecules occupy adsorption sites on the coal surface, thereby weakening the coal's ability to adsorb water molecules and reducing its wettability. However, under these conditions, the coal generally remains in a water-wet state. In contrast, under high-pressure CO_2 conditions, except for the low-rank HQ coal, the contact angles on the coal surface exceed 90°, indicating a wettability reversal—from water-wet to gas-wet behavior. This reversal is attributed to the significant increase in CO_2 adsorption with pressure, which leads to larger contact angles and a transition of the coal surface from hydrophilic to hydrophobic. At the same pressure, contact angles in CO_2 environments are consistently larger than those in CH_4 environments. Moreover, the number of hydrogen bonds in CH_4 systems is consistently higher than in CO_2 systems, indicating that CH_4 has a weaker effect on coal surface wettability compared to CO_2. Specifically, the simulated contact angle for DP coal at 5 MPa CO_2 (76.09°) demonstrates close quantitative matching with the experimental value of 78° reported by Siemons et al. [20]. Additionally, the pressure-induced increase in contact angles within CO_2 systems exhibits trend consistency with the NMR results of Zheng et al. [4], who observed stabilization at 5 MPa. Furthermore, the decreasing trend of hydrogen bond counts with increasing pressure (as shown in Table 6) correlates well with the experimental reduction in water adsorption measured by Yue et al. [33]. Siemons et al. [20] experimentally observed that the contact angle in a coal–CO_2–water system increases with pressure, which aligns well with our simulation finding that contact angles rise with pressure, particularly in CO_2 environments.

To further investigate the molecular mechanism underlying these differences, the HQ coal system was used to analyze the density distributions of CH_4-H_2O and CO_2-H_2O under pressures of 2.5, 5.0, 7.5, and 10.0 MPa at 298 K (Figures 16 and 17). The corresponding peak density values for each gas–water pair at different pressures are summarized in Table 8. These analyses provide molecular-level insights into how the nature of the injected gas influences coal wettability.

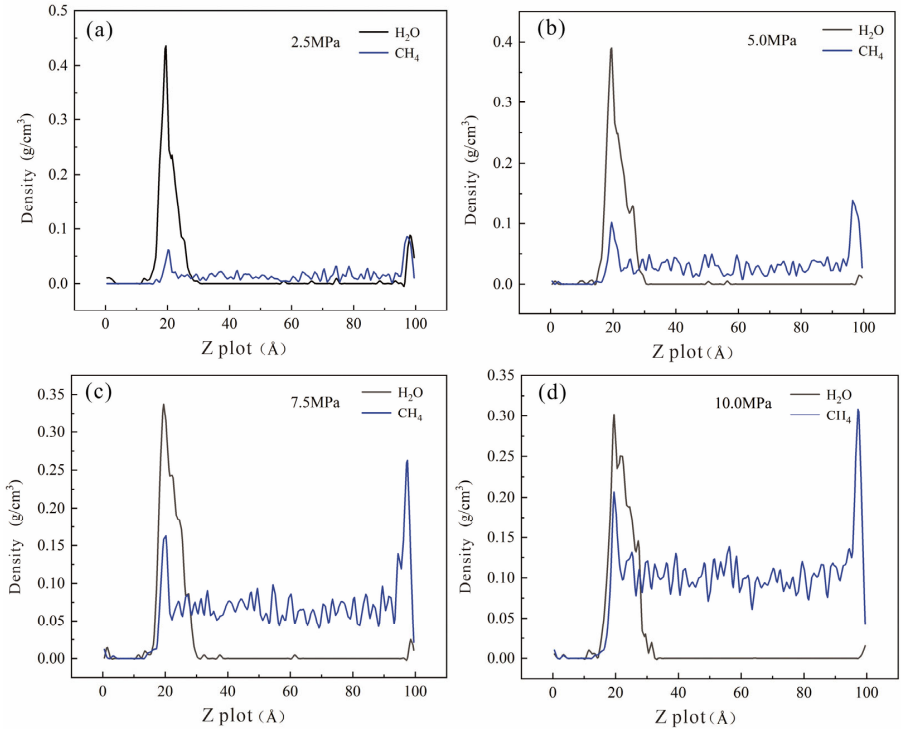

Figure 16. Molecular density curves at different CH_4 gas pressures. (**a**) 2.5 MPa; (**b**) 5.0 MPa; (**c**) 7.5 MPa; (**d**) 10.0 MPa.

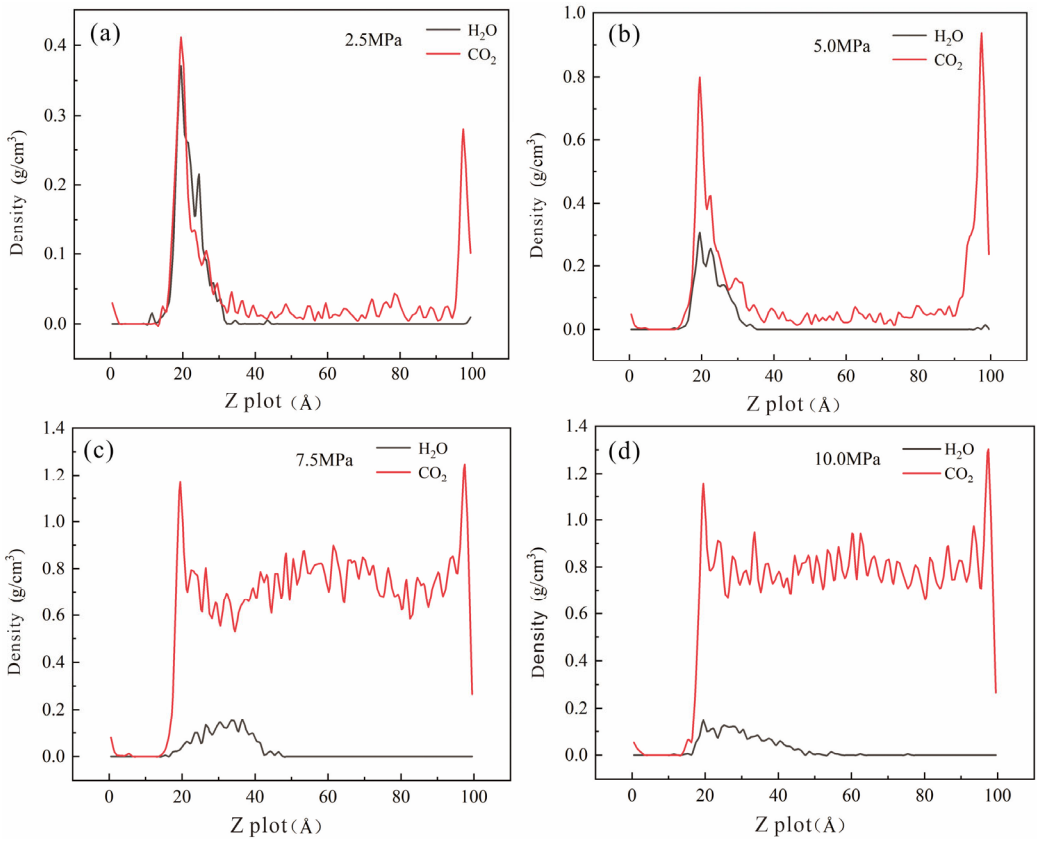

Figure 17. Molecular density curves at different CO_2 gas pressures. (**a**) 2.5 MPa; (**b**) 5.0 MPa; (**c**) 7.5 MPa; (**d**) 10.0 MPa.

Table 8. Molecular density characteristics in the HQ coal system under different gas environments at 298 K.

	CH_4 Environment		CO_2 Environment	
Pressure (MPa)	**CH_4 Density (g/cm^3)**	**H_2O Density (g/cm^3)**	**CO_2 Density (g/cm^3)**	**H_2O Density (g/cm^3)**
2.5	0.061	0.436	0.411	0.370
5	0.102	0.390	0.798	0.308
7.5	0.158	0.337	1.15	0.156
10	0.207	0.302	1.17	0.146

As shown in Table 8, at a constant temperature of 298 K and pressures ranging from 2.5 MPa to 10.0 MPa, with coal rank Ro between 0.67% and 2.21%, the maximum water density in the coal–water–CH_4 system decreases from 0.436 g/cm^3 to 0.302 g/cm^3. In the coal–water–CO_2 system, the water density drops even more significantly, from 0.370 g/cm^3 to 0.146 g/cm^3, indicating a reduction in the number of water molecules adsorbed on the coal surface. As shown in Figures 16 and 17, the density distribution curves of water molecules broaden and exhibit more peaks with increasing pressure, suggesting a shift in water adsorption behavior from concentrated and ordered to dispersed and disordered. This change reflects a weakened ability of the coal surface to adsorb water, as well as a loss of compactness and stability in the adsorbed water layer. As a result, water molecules are unable to aggregate effectively at the coal surface, leading to decreased wettability. Under identical conditions, changes in the water density distribution curves are more pronounced in the CO_2 environment, indicating a more significant deterioration of wettability. This is because, at higher pressures, a dense layer of CO_2 molecules forms on the coal surface, occupying adsorption sites and exerting repulsive and disruptive effects

on water molecules. These effects hinder the approach of water molecules and inhibit the formation of stable hydrogen bonds. Consequently, water density distributions shift from sharp, concentrated peaks to broader, multi-peak patterns with lower peak intensities, reflecting the disintegration of the adsorbed water layer and a substantial decline in coal wettability. In contrast, the disturbance caused by CH_4 is relatively mild, resulting in smaller changes in water density and less degradation of wettability.

As shown in Figure 18, under increasing pressure in the CH_4 environment, the CH_4 density peak rises slowly, while the water density peak gradually decreases; both changes remain moderate. In the CO_2 environment, however, the CO_2 density peak increases sharply with pressure, greatly exceeding the water density and showing a clear crossover trend, especially above 7.5 MPa. This indicates that under high-pressure CO_2, more CO_2 molecules enter the coal pores and occupy adsorption sites, preferentially adsorbing onto the internal surfaces and displacing water molecules. This competitive adsorption leads to a rapid decline in water density and a corresponding deterioration in coal surface wettability. Compared to CO_2, CH_4 exhibits a slower increase in density and exerts weaker repulsive effects on water, resulting in less pronounced wettability changes. This contrast clearly demonstrates that the nature of the injected gas significantly influences coal wettability at the molecular scale, with CO_2 exhibiting a much stronger inhibitory effect and causing more severe degradation in wettability.

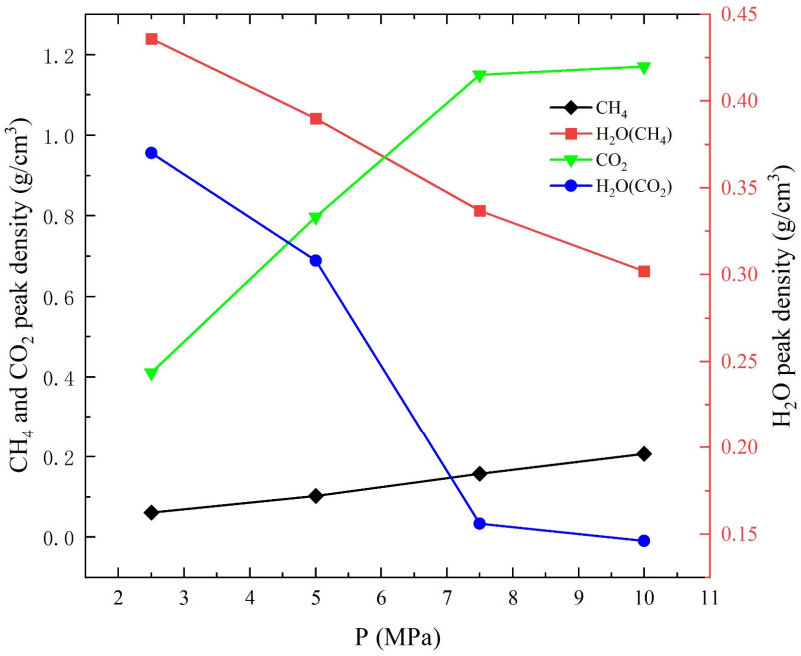

Figure 18. Changes in molecular density peaks under different gas pressures.

4.4. Correlation Analysis of Wettability Across Different Coal Ranks

To investigate the differences in wettability among coal ranks, the contact angle, number of hydrogen bonds, and the abundance of oxygen-containing functional groups for each coal macromolecular model were quantified under conditions of 5 MPa and 298 K (Table 9). Subsequently, Pearson correlation analysis was performed using Origin software v8.5 to evaluate the relationships among these parameters. The resulting correlation heatmaps for coal wettability under different gas environments are shown in Figure 19.

Table 9. Correlation-related parameters of coal wettability under different gas environments across coal ranks.

Sample	HQ	DP	GY	ZZ
R_O	0.67	1.50	1.96	2.21
Contact angle in CH_4 (°)	41.17	75.02	77.03	84.24
Contact angle in CO_2 (°)	44.9	76.09	77.73	90.15
Hydrogen bonds in CH_4	84	6	10	8
Hydrogen bonds in CO_2	74	6	9	6
Carbonyl groups (C=O)	2	0	1	1
Carboxyl groups (–COOH)	2	0	0	0
Hydroxyl groups (–OH)	28	2	1	1
Ether oxygen groups (–O–)	2	0	1	3
Aldehyde groups (–CHO)	0	1	0	0

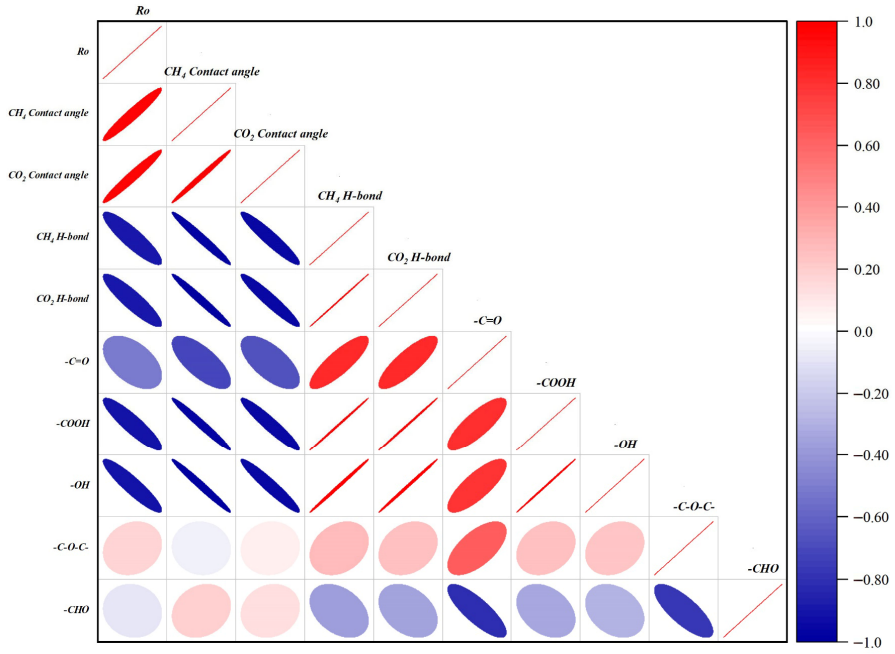

Figure 19. Heatmaps of coal wettability correlations across different coal ranks under gas environment: CH_4 environment and CO_2 environment.

As shown in Table 9, with increasing coal rank, the number of polar functional groups such as –OH and –COOH in the coal macromolecules decreases significantly. This reduction in polarity impairs the coal surface's ability to form hydrogen bonds with water molecules. Since hydrogen bonding enhances the interaction between water and the solid surface—facilitating droplet spreading—a decrease in hydrogen bond formation directly leads to larger contact angles and reduced wettability. The low-rank HQ coal forms the highest number of hydrogen bonds with water and exhibits the smallest contact angle, indicating strong hydrophilicity. In contrast, the high-rank ZZ coal has very few hydrogen bonds, in some cases approaching zero, resulting in poor water adsorption on the surface and a significantly increased contact angle. Under high-pressure CO_2 conditions, this even leads to a wettability reversal from water-wet to gas-wet behavior. In low-rank coals, the abundance of polar functional groups helps maintain wettability, making it less sensitive to gas-induced disturbance. However, in high-rank coals, the inhibitory effect of gas molecules—especially CO_2—on water adsorption becomes more pronounced, amplifying the wettability differences across coal ranks. As illustrated in Figure 19, there is a strong negative correlation between contact angle and both the number of hydrogen bonds and

the content of polar functional groups. In contrast, a strong positive correlation exists between contact angle and coal rank. This indicates that with coalification, the surface polarity of coal decreases, reducing its ability to form hydrogen bonds with water, thereby increasing the contact angle and weakening wettability. This trend is particularly evident under CO_2 environments, where wettability differences are further magnified, and some high-rank coals exhibit a transition from hydrophilic to hydrophobic behavior. Overall, the degree of coalification governs the evolution of surface chemical structures, which in turn controls the coal's ability to adsorb water molecules and ultimately determines its wettability characteristics.

Additionally, as shown in Table 9, under the same temperature and pressure conditions, the contact angle of HQ coal is significantly lower than that of the other three coals in both CO_2 and CH_4 environments. Low-rank coals (e.g., HQ coal with Ro = 0.67%) exhibit abundant –OH groups (28 per molecule, as shown in Table 2), forming dense hydrogen bond networks with water molecules. This structural feature maintains a robust hydration layer even at elevated temperatures (298–338 K), evidenced by the minimal change (<2°) in contact angles for HQ coal across temperatures in both CH_4 and CO_2 environments—markedly contrasting with the 10–20° reductions in mid- and high-rank coals (Table 5). Additionally, HQ coal retains about 74% of its hydrogen bonds at 338 K relative to 298 K, far exceeding the 60% retention in high-rank ZZ coal (Table 6). The –OH groups act as "thermal buffers" via two mechanisms: enhancing hydration stability through multiple hydrogen bonds that resist thermal disruption (supported by molecular dynamics showing reduced root-mean-square displacement of water molecules near –OH groups at high temperatures) and reducing gas adsorption sensitivity, with CO_2 density decreasing by only 6.3% in HQ coal versus 20.4% in ZZ coal from 298 K to 338 K (Table 7), thus prioritizing water adsorption. In contrast, the decline in –OH content with increasing coal rank weakens hydrogen bonding, leading to more pronounced temperature-dependent wettability and greater water surface tension decreases. These findings imply reduced effectiveness of CO_2-ECBM in low-rank coals at high temperatures due to water retention and improved water-based heat transfer in low-rank coal geothermal systems. Future research may involve in situ thermal experiments, deuterated water isotope tracing, and multi-component system studies to validate these mechanisms.

5. Conclusions

Molecular dynamics simulations were performed to assess the wettability of four coal samples of varying ranks (HQ, DP, GY, ZZ) under different temperature and pressure conditions. The key findings are summarized as follows:

(1) Higher gas pressure enhanced CH_4 and CO_2 adsorption on the coal surface, reducing hydrogen bonding with water and increasing contact angles. In high-pressure CO_2 environments (>5 MPa), most high-rank coals exhibited wettability reversal from water-wet to gas-wet. CH_4 had a milder effect due to weaker adsorption.

(2) Elevated temperature increased water molecule mobility and gas desorption, freeing up adsorption sites for water. This promoted hydrogen bond formation and reduced surface/interfacial tension, thereby improving wettability—especially in high-rank coals.

(3) CO_2, due to its higher polarity and stronger surface affinity, adsorbed more readily than CH_4, occupying critical sites and disrupting water adsorption and hydrogen bonding. This led to more diffuse water density distributions and poorer wettability compared to CH_4.

(4) Wettability was strongly positively correlated with coal rank and negatively correlated with hydrogen bond count and polar functional group content. As coal rank increased,

the reduction in surface polarity weakened water adsorption, especially under CO_2, promoting wettability reversal.

Author Contributions: L.Z.: investigation, conceptualization, methodology, software, writing—original draft preparation, data, and validation. S.Z.: conceptualization, methodology, data, validation, resources, writing—review and editing, supervision, project administration, and funding acquisition. S.T.: supervision and writing—review and editing. Z.X.: supervision and writing—review and editing. J.L.: software and validation. Q.Z.: supervision and visualization. K.Z.: supervision and visualization. W.T.: supervision and investigation. All authors have read and agreed to the published version of the manuscript.

Funding: The project is funded by the National Natural Science Foundation of China (Nos: 42472235 and 42430805) and the tackling applied science and technology projects of the China National Petroleum Corporation (2023ZZ18YJ01).

Data Availability Statement: The research data of this article can be obtained from the author "Lixin Zhang" through reasonable request.

Conflicts of Interest: Author Wenguang Tian was employed by Research Institute of Petroleum Exploration and Development, PetroChina. The remaining authors declare that the research was conducted in the absence of any commercial or financial relationships that could be construed as a potential conflict of interest.

References

1. Yao, Y.; Liu, D.; Xie, S. Quantitative Characterization of Methane Adsorption on Coal Using a Low-Field NMR Relaxation Method. *Int. J. Coal Geol.* **2014**, *131*, 32–40. [CrossRef]
2. Yao, Y.; Liu, D. Rock Physics and Fluid Characterization of Coal Reservoirs Based on NMR Relaxation Spectra. *Coal Sci. Technol.* **2016**, *44*, 14–22. [CrossRef]
3. Sun, X.; Yao, Y.; Liu, D.; Zhou, Y. Investigations of CO_2-Water Wettability of Coal: NMR Relaxation Method. *Int. J. Coal Geol.* **2018**, *188*, 38–50. [CrossRef]
4. Zheng, S.; Yao, Y.; Elsworth, D.; Liu, D.; Cai, Y. Dynamic Fluid Interactions During CO_2-ECBM and CO_2 Sequestration in Coal Seams. Part 2: CO_2-H_2O Wettability. *Fuel* **2020**, *308*, 279. [CrossRef]
5. Sun, X.; Yao, Y.; Chen, J.; Xie, S.; Li, C. Analysis of Coal Wettability Based on Low-Field Nuclear Magnetic Resonance. *Mod. Geol.* **2015**, *29*, 190–197. [CrossRef]
6. Yao, Y.; Sun, X.; Wan, L. Research on the Micro-Mechanism of CO_2 Geological Sequestration in Coal Seams. *Coal Geol. Explor.* **2023**, *51*, 146–157. [CrossRef]
7. Li, J. Analysis of Factors Affecting Coal Surface Wettability. Master's Thesis, Henan Polytechnic University, Jiaozuo, China, 2016.
8. Li, J.; Li, K. Factors Affecting Coal Surface Wettability. *J. China Coal Soc.* **2016**, *41* (Suppl. S2), 448–453. [CrossRef]
9. Li, S.; Guo, D.; Bai, Y.; Yan, M.; Lin, H.; Shi, Y. Molecular Simulation of the Effect of Different Mass Fractions of SDBS on Coal Wettability. *China Saf. Sci. J.* **2020**, *30*, 21–27. [CrossRef]
10. Xu, Y.; Li, P.; Sun, Z. Study on the Influencing Factors of Wettability of Coal Dust of Different Metamorphic Degrees. *Coal Mine Mach.* **2022**, *43*, 65–68. [CrossRef]
11. Gao, M.; Wang, M.; Xie, J.; Gao, Y.; Deng, G.; Yang, B.; Wang, F.; Hao, H.; Xie, H. Research on In-Situ Disturbance Mechanical Behavior of Deep Coal Rock. *J. China Coal Soc.* **2020**, *45*, 2691–2703. [CrossRef]
12. Li, M.; Xu, H.; Shu, X. Discussion on the Application of Chemical Dust Suppressants in Coal Dust Suppression. *China Coal* **2007**, 46–47+50. [CrossRef]
13. Shi, X.; Jiang, Z.; Deng, Y.; Xing, J. Study on Dust Pollution in Fully Mechanized Mining Face. *J. Saf. Sci. Technol.* **2008**, *4*, 67–70. [CrossRef]
14. Yuan, L. Scientific Conception of Coal Mine Dust Control and Occupational Safety and Health. *J. China Coal Soc.* **2020**, *45*, 1–7. [CrossRef]
15. Wang, J. Experimental Study on Physicochemical Characteristics and Dust Reduction of Coal Dust of Different Particle Sizes. Ph.D. Thesis, China University of Mining and Technology, Beijing, China, 2019.
16. Zhang, J.; Li, H.; Liu, Y.; Li, X.; Xie, J.; Dai, Z.; Ye, S.; Li, L.; Zhou, W.; Zhao, Y.; et al. Microcosmic Wettability Characteristics of Coal Dust and Preliminary Exploration of Dust Suppressant Development: A Case Study of Pingdingshan Mining Area. *J. China Coal Soc.* **2021**, *46*, 812–825. [CrossRef]

17. Yan, M.; Yue, M.; Lin, H.; Yan, D.; Wei, J.; Qin, X.; Zhang, J. Experimental Study on the Influence of Functional Groups on the Wettability of Medium and Low Rank Coal. *Coal Sci. Technol.* **2023**, *51*, 103–113. [CrossRef]
18. Zhou, G.; Cheng, W.; Xu, C.; Nie, W. Analysis of ^{13}C-NMR Characteristics of Wettability Differences of Coal Dust of Different Metamorphic Degrees. *J. China Coal Soc.* **2015**, *40*, 2849–2855. [CrossRef]
19. Zhou, G.; Xue, J.; Cheng, W.; Nie, W.; Wang, H. Influence of Stacking Structure on Coal Dust Wettability Based on X-Ray Diffraction Experiment. *Chin. J. Eng.* **2015**, *37*, 1535–1541. [CrossRef]
20. Siemons, N.; Bruining, H.; Castelijns, H.; Wolf, K.-H. Pressure Dependence of the Contact Angle in a CO_2-H_2O-Coal System. *J. Colloid Interface Sci.* **2006**, *297*, 755–761. [CrossRef] [PubMed]
21. Chen, J.; Yao, Y.; Sun, X.; Xie, S.; Guo, W. Study on the Influence of CO_2 and Helium on the Wettability of Low-Rank Coal. *Coal Sci. Technol.* **2015**, *43*, 129–134. [CrossRef]
22. Xia, Y.; Yang, Z.; Zhang, R.; Xing, Y.; Gui, X. Enhancement of the Surface Hydrophobicity of Low-Rank Coal by Adsorbing DTAB: An Experimental and Molecular Dy-namics Simulation Study. *Fuel* **2019**, *239*, 145–152. [CrossRef]
23. Van Niekerk, D.; Mathews, J.P. Molecular Dynamic Simulation of Coal-Solvent Interactions in Permian-Aged South African Coals. *FPT* **2011**, *92*, 729–734. [CrossRef]
24. Zhao, Y.; Li, H.; Lei, J.; Xie, J.; Li, L.; Gan, Y.; Deng, J.; Qi, R.; Liu, Y. Study on the Surface Wetting Mechanism of Bituminous Coal Based on the Microscopic Molecular Structure. *RSC Adv.* **2023**, *13*, 5933–5945. [CrossRef] [PubMed]
25. Li, E.; Lu, Y.; Cheng, F.; Wang, X.; Miller, J.D. Effect of Oxidation on the Wetting of Coal Surfaces by Water: Experimental and Molecular Dynamics Simulation Studies. *Physicochem. Probl. Miner.* **2018**, *54*, 1039–1051.
26. Meng, J.; Wang, L.; Zhang, S.; Lyu, Y.; Xia, J. Effect of Anionic/Nonionic Surfactants on the Wettability of Coal Surface. *Chem. Phys. Lett.* **2021**, *785*, 139130. [CrossRef]
27. Xia, Y.; Rong, G.; Xing, Y.; Gui, X. Synergistic Adsorption of Polar and Nonpolar Reagents on Oxygen-Containing Graphite Surfaces: Implications for Low-Rank Coal Flotation. *J. Colloid Interface Sci.* **2019**, *557*, 276–281. [CrossRef] [PubMed]
28. Liu, N. Experimental Study on Competitive Wetting Characteristics of CO_2 and Water in Coal of Different Metamorphic Degrees Under High Temperature and High Pressure. Master's Thesis, China University of Mining and Technology, Beijing, China, 2022. [CrossRef]
29. Zhang, C.; Zhang, S.; Tang, S.; Zhang, S.; Li, Z.; Fan, Z. Construction and Comparison of Coal Macromolecular Models of Different Ranks. *Mod. Geol.* **2025**, *39*, 839–855. [CrossRef]
30. Zhang, C.; Zhang, S.; Tang, S.; Zhang, S.; Li, J. Study on the Wetting Mechanisms of Different Coal Ranks Based on Molecular Dynamics. *Processes* **2024**, *12*, 455. [CrossRef]
31. Sakamaki, R.; Sum, A.K.; Narumi, T.; Yasuoka, K. Molecular dynamics simulations of vapor/liquid coexistence using the nonpolarizable water models. *J. Chem. Phys.* **2011**, *134*, 124708. [CrossRef]
32. Si, L.; Gu, Y.; Wei, J.; Ding, N.; Jiang, W.; Yao, B.; Wen, Z. Variation Law and Microscopic Interaction Mechanism of Coal-Water Wettability Dynamic Spreading under Different Gas Environments. *J. China Coal Soc.* **2025**, 1–16. [CrossRef]
33. Yue, J.; Wang, C.; Shi, B.; Wang, Z.; Xu, J.; Han, Q.; Sun, Y.; Liang, Y. Wettability Characteristics and Influencing Mechanisms of Coal-Water Interface Under Methane Atmosphere. *J. China Coal Soc.* **2024**, *49*, 4325–4335. [CrossRef]

Disclaimer/Publisher's Note: The statements, opinions and data contained in all publications are solely those of the individual author(s) and contributor(s) and not of MDPI and/or the editor(s). MDPI and/or the editor(s) disclaim responsibility for any injury to people or property resulting from any ideas, methods, instructions or products referred to in the content.